

Assessment of complex rock slope stability at Xiari, southwestern China

Changqing Qi¹ · Jimin Wu¹ · Jin Liu¹ · Debi Prasanna Kanungo²

Received: 3 December 2014 / Accepted: 13 June 2015 / Published online: 30 June 2015
© Springer-Verlag Berlin Heidelberg 2015

Abstract Detailed engineering geological studies and stability assessments were carried out on Xiari rock slope in southwestern China. Geomorphic analysis of digital elevation models, detailed structural field mapping and boreholes data indicate that the slope has a poor rock mass quality and complex deformation mechanism. The necessary rock mass parameters were determined by means of slope mass rating (SMR), geomechanic classification system (Q) and geological strength index (GSI). Slope stability analyses were performed by means of kinematic, limit equilibrium and numerical modeling techniques. Analyses results indicate that slope stability is mainly controlled by the discontinuities. The combination of discontinuities and topography makes the slope susceptible for a large landslide. The major potential mode of slope failure is planar failure. Planar failure has a higher probability in comparison to wedge failure, while wedge failure contributes towards a more severe hazard, like the landslide in part A of the study area. Numerical analysis results indicate a catastrophic landslide in the future, with a volume estimated to be more than $2.5 \times 10^6 \text{ m}^3$.

Keywords Rock slope stability · Engineering geology · Rock classification system · Failure mechanism · Landslide · Numerical modeling

Introduction

The plentiful water resources and stepped terrains between the Tibetan Plateau and Sichuan Basin are very favorable for hydropower exploitation. But the narrow and steep valleys in this area are prone to large-scale slope failures (Huang 2009). Historical records and geological studies show numerous large rock slides and slope instabilities in this setting (Wen et al. 2004; Dai et al. 2005; Huang 2009; Yin et al. 2009; Zhou et al. 2010; Huang and Fan 2013; Xu et al. 2013). One of the catastrophic landslides, the Tanggudong landslide, occurred in 1967 and was located on the right bank of Yalong River Valley in Yajiang City of Sichuan Province, situated merely 3.5 km upstream of the study area. Having poor rock mass integrity and unfavorable discontinuities, Xiari rock slope is considered to be one of the major potential geological hazards in this area today. The slope, downstream of the village Xiari, covers an area of about 1.6 km^2 that extends 1.2 km downstream and 1.3 km upslope, showing complex topography and different deformation indications (Fig. 1). Yalong River is China's third largest hydropower base and 21 cascade projects have been planned along this river (Wu et al. 2010). One of the proposed hydropower projects is located just downstream of Xiari slope. Due to the huge threat to the proposed hydropower station, the stability and potential deformation behavior of this slope has drawn great attention.

In order to understand the stability and possible deformation mechanism of a complex rock slope like Xiari, the integration of geological, geotechnical and modeling techniques is needed (Böhme et al. 2013). Field investigation and laboratory tests can provide basic information about slope structure and characteristics. This information is essential for developing a geomechanical model. Rock mass classification systems are useful tools for estimating

✉ Changqing Qi
qichangqing79@gmail.com

¹ School of Earth Sciences and Engineering, Hohai University, Nanjing 210098, China

² CSIR-Central Building Research Institute (CBRI), Roorkee 247667, India

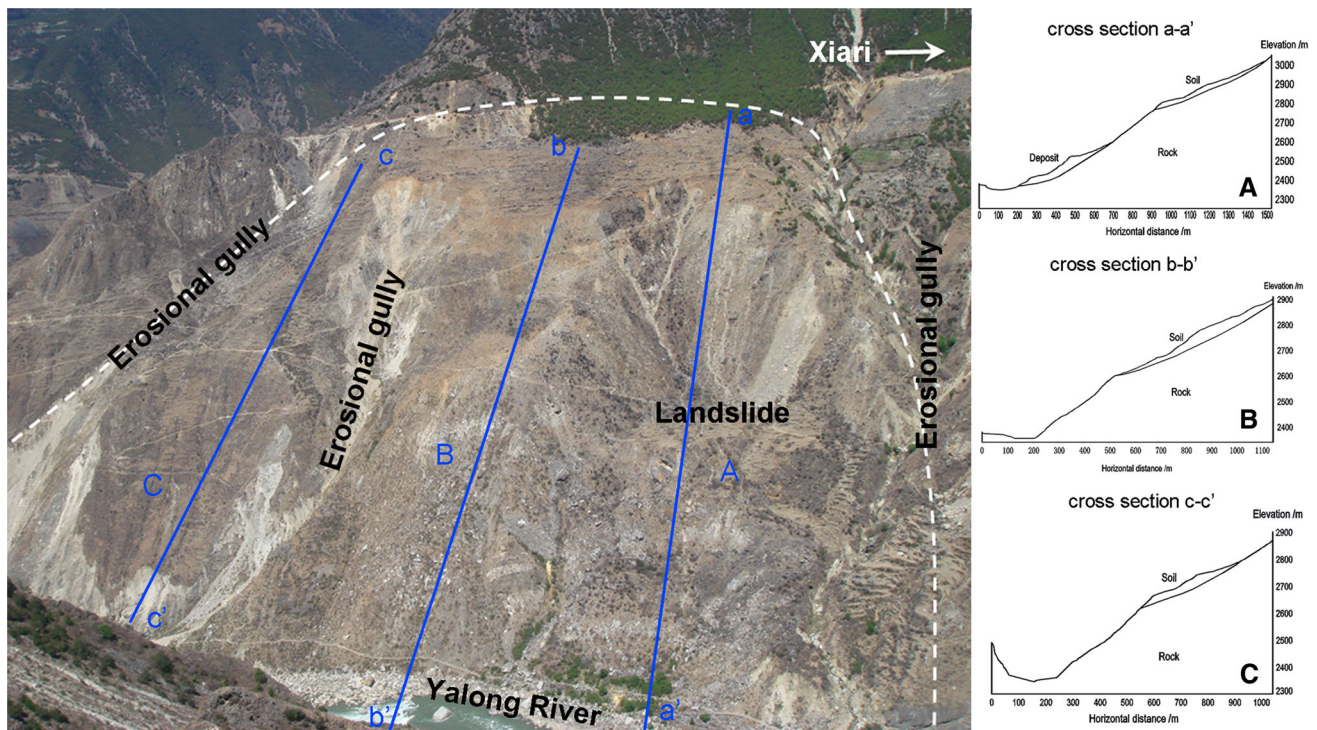


Fig. 1 View of Xiari slope in the Yalong River Valley. The boundary of the study area and cross sections are also shown

rock mass quality and properties, which are especially important for jointed rock mass (Genis et al. 2007; Justo et al. 2009). Kinematics, limit equilibrium and numerical modeling techniques are commonly used methods for rock slope stability analysis (Gurocak et al. 2008). Kinematic models are easy and helpful methods for stability analysis of jointed rock slopes. But the kinematic analyses are oversimplified and are often used for a first-hand assessment of the slope stability (Stead et al. 2006; Gurocak et al. 2008). For a thorough understanding of the deformation mechanisms of the slopes and for estimating the failure dimensions, numerical modeling techniques are useful.

The scope of this paper is to characterize the principal instability mechanisms potentially affecting Xiari rock slope. To achieve this, detailed structural field mapping, topographic analysis using a digital elevation model (DEM) and characterization of rock mass properties have been carried out. In addition, kinematic analysis, limit equilibrium probability analysis and numerical modeling analysis were also adopted to understand the failure mechanism, failure probability, and the potential failure dimensions of the unstable slope.

Geological setting

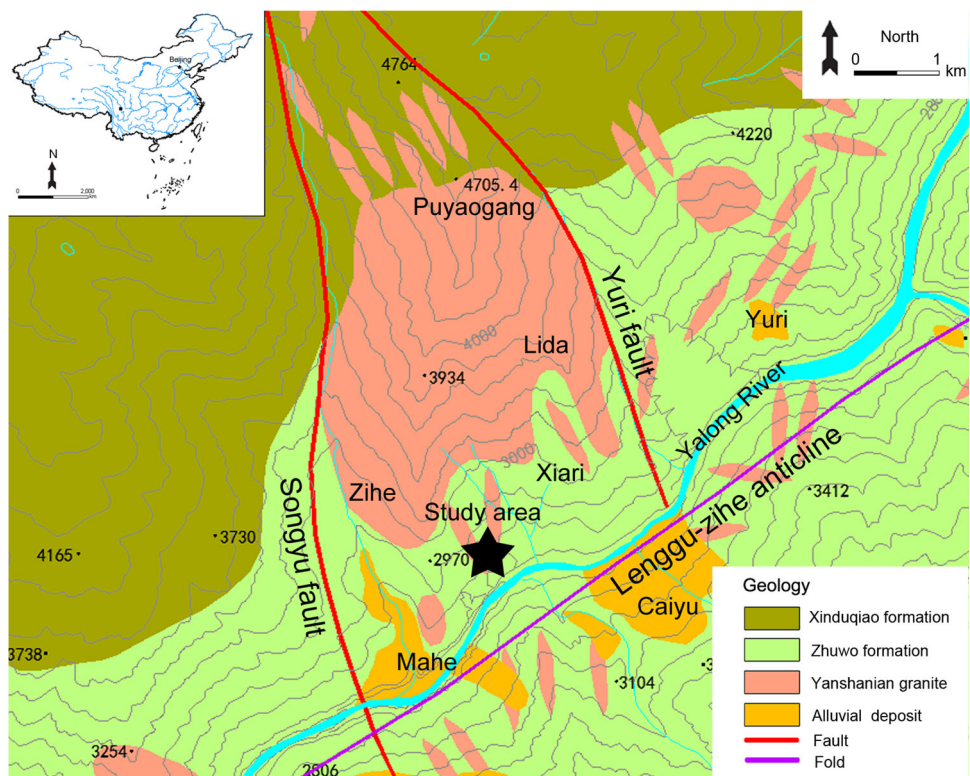
The study area is situated towards the east of the Qinghai-Tibet Plateau, where the altitude decreases sharply from the west to the east. The valley is narrow and steep with an

asymmetric V shape. The Yalong River meanders through the study area in a direction from N60°W towards S30°W (Fig. 2). The water level in the Yalong River at the study location is at an elevation of about 2340 m.

The exposed bedrock in the area consists mainly of lower Mesozoic metamorphic rocks and Yanshanian granite. The more important lithological units are the upper Triassic Xiduqiao and Zhuwo formations. The former forms the upper part of the slope and the latter forms the lower part (Fig. 2). The Xinduqiao formation comprises mainly dark gray shale and the Zhuwo formation comprises low-grade metamorphic sandstone. The metamorphic sandstone is grey in color and has intermediate to thick layering. The granite, recognized as fine-grained biotite granite, intrudes as stocks and dikes. During the Himalayan orogeny, the rocks were intensively reworked by the collision between India and Eurasia that resulted in rapid uplifting of Qinghai-Tibet Plateau in the Quaternary period. The high tectonic stress, in addition to heavy unloading caused by fast river erosion, has resulted in a large number of deep cracks in Southwestern China (Qi et al. 2004; Gong et al. 2010). The unstable slope under study is situated directly at the foot of the granite stock. The intrusion of magma is likely to have changed the stress pattern of the slope and caused different deformation behavior during late tectonic activities, and thus might explain the instability exactly at this site.

The most evident structure in the area is the Lenggu-zihe anticline. It has an asymmetrical form, with a

Fig. 2 Geological settings plotted on elevation contours of the study area



southeasterly plunge. The study area is located near the core of the anticline, situated on the northwestern limb (Fig. 2). Two faults, Songyu fault and Yuri fault, lie downstream and upstream of Xiari slope, respectively.

Engineering geological appraisal of Xiari rock slope

Xiari unstable rock slope is located on the northern slope of Yalong River Valley. The height of the unstable slope is about 750 m, with an elevation of 2350 m at the foot of the slope. The whole slope orientation is about N140°/40°. A digital elevation model was constructed based on a contour map of 1:5000 scale with a contour interval of 5.0 m (Fig. 3). It can be seen that Xiari slope is situated just between two large gullies, where the upstream gully is deeper and steeper. The upper part of the slope is covered by debris deposit and has a gentle slope angle of less than 25°. The lower terrain of the slope is steep (about 40°) with exposed bedrock. According to the topography and deformation characteristics, we divided the lower part of the slope into three subareas. The upstream part, subarea A, includes a landslide of unknown age. The landslide shows a structurally controlled failure mode. The landslide slipped towards the outlet of upstream gully. The main scarp of the landslide is steep with exposed bedrock. At the top of the

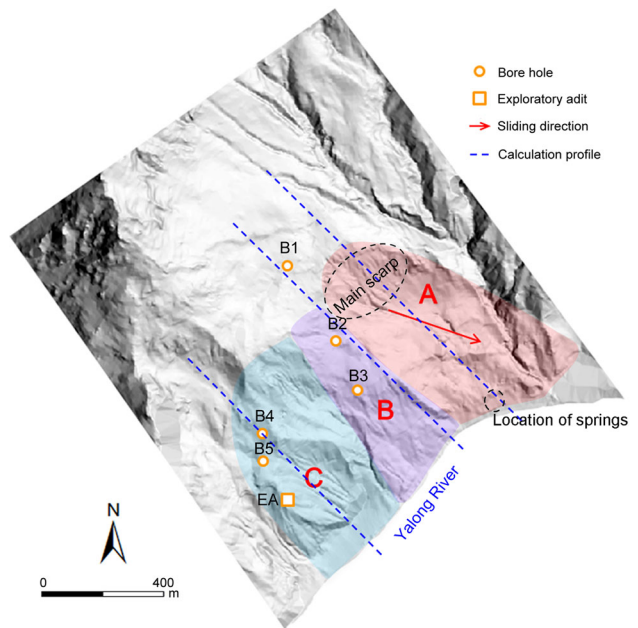


Fig. 3 Digital elevation model of Xiari slope: A, B and C are the three subareas discussed in this paper; B1–B5 are the locations of bore holes; EA is the location of the exploratory adit; the three dotted lines are the profile sections for stability analysis

scarp, transverse cracks and minor scarps can be found in the deposit. At the toe of the landslide deposit, several landslide springs can be found. The central part of the

slope, subarea B, is mostly covered by the collapsed deposit. The bedrock exposed here is fractured. Some freestanding blocks split by discontinuities were observed in this area (Fig. 4). The downstream part, subarea C, is convex with a cliff-like toe. This part shows a different deformation pattern. Rock avalanche deposit was found near the toe of the subarea C (Fig. 5). Between the subareas B and C, an erosional gully has developed.

Most part of the slope surface is covered by debris deposit. Discontinuity planes at 112 different locations were measured, mostly in the subarea C. The poles of these discontinuities were plotted, contoured and four major joint sets were derived on equal-area stereographic projection plot (Fig. 6). The orientation of these joints, which were given as dip direction and dip angle in degrees, are N124°/31° (J_1), N221°/73° (J_2), N136°/60° (J_3) and N294°/51° (J_4). The spacing of joint sets J_1 to J_3 ranges between 0.1 and 0.5 m. Joint set J_4 runs parallel to the bedding plane with spacing varying from 0.2 to 0.6 m. The discontinuities are moderately to highly persistent, and the joints walls are smooth and undulating in metamorphic sandstone and rough in granite according to the International Society for Rock Mechanics (ISRM) (1981). The volumetric joint count was estimated to be 30 using the empirical relationship provided by Palmstrom (2005).

Field observations indicated that the mode of existing failures and deformation of the slope are strongly influenced by the combination of different joint sets. The basal failure surface of the landslide in subarea A was observed to be developed along J_1 , where J_2 and J_3 served as lateral and rear separate structures. Unstable toppled blocks in subarea B were also delimited by the combination of joint sets J_1 , J_2 and J_3 (Fig. 4).



Fig. 4 Loose rock blocks observed in subarea B

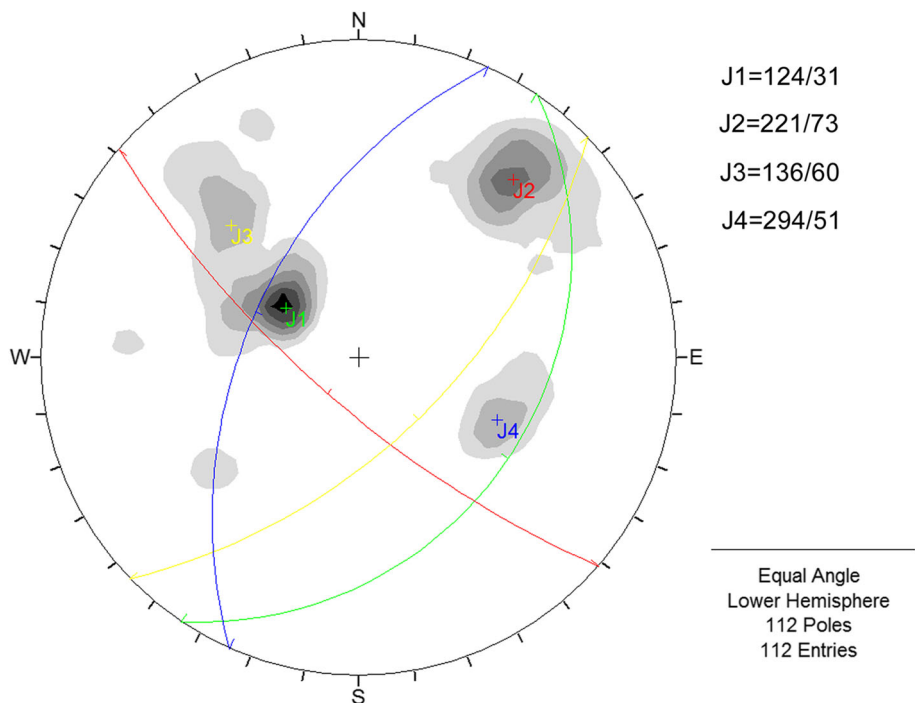


Fig. 5 Rock avalanche at the toe of subarea C

Five boreholes and an exploratory adit were made in the study area to thoroughly understand the structure and rock mass quality of the slope. The locations of the boreholes and exploratory adit are shown in Fig. 3. The boreholes were vertically drilled. The top elevations of boreholes B1 to B5 were 2848, 2716, 2597, 2638, and 2606 m, and the corresponding depths were 140.8, 101.5, 60.6, 100.7 and 112.4 m, respectively. The exploratory adit was about 200 m long in horizon at the elevation of 2532 m. Borehole data detected that the depth of overlying soil varies from a minimum of 4.3 m at borehole B3 to a maximum of 35.2 m at borehole B1. The underlying rock mass was observed to be highly weakened by unloading and tectonic movement. Many crushed zones were observed in drilled cores. The rock quality designation (RQD) of the rock obtained from boreholes B1 to B5 are 14, 13, 16, 14 and 31 %, respectively, with an average value of 17.6 %. The in situ rock mass was consequently identified as being of very poor quality (Deere 1989).

Borehole and adit data detected that granite dikes occur alternately with metamorphic sandstone. The thickness of granite dikes varies from several meters to dozens of meters. The granite is moderately weathered and crushed. The crushed blocks on the adit ceiling cannot maintain its stability without simple support. The uniaxial compressive strength of granite varies from 35 to 77 MPa with an average of 56 MPa. The average elastic modulus of intact granite is 30 GPa. The metamorphic sandstone revealed in the test pit is slightly weathered. The uniaxial compressive strength of metamorphic sandstone varies from 63 to 117 MPa, with an average of 90 MPa. The average elastic modulus of intact metamorphic sandstone is 39 GPa. Several cracks (within the distance from the adit entrance to a depth about 180 m) and small shear faults along joint

Fig. 6 Density stereo plot of the discontinuities data collected from field and the derived mean surfaces for the major discontinuity sets



set J_3 were observed in the exploratory adit. The deep cracks and shear faults were typical structures caused by the combination effect of tectonic movement and unloading (Qi et al. 2004). The rock mass was completely dry in the exploratory adit and none of the boreholes intercepted a water table.

Estimating rock mass properties

The strength parameters and/or deformation modulus are fundamental input parameters for numerical modeling. For jointed rock mass, these parameters mainly depend upon the joint pattern. So, the parameters obtained from laboratory tests on core samples are not logically used in a numerical model that compares with those from the comprehensive classification systems (Justo et al. 2009). In this paper, rock slope stability classification systems such as slope mass rating (SMR) (Romana 1985), Q (Barton 2002) and geological strength index (GSI) (Hoek 1994; Hoek et al. 1995) were employed to characterize the rock mass and to estimate the rock mass strength parameters.

Rock mass classifications

Rock Mass Rating (RMR) geomechanics classification (Bieniawski 1973) has become a standard for use in rock mass engineering. The basic RMR value incorporates five parameters: strength of intact rock, rock quality designation (RQD), spacing of joints, condition of joints and

groundwater conditions. But rating adjustments for discontinuities orientation for slopes are relatively rough and difficult to quantitatively definite. So Romana (1985) extended the RMR system to the SMR system for use in rock slope engineering. The SMR value is obtained by adjusting the basic RMR value with orientation of joints and slopes and excavation adjustments for slopes:

$$SMR = RMR + (F_1 \cdot F_2 \cdot F_3) + F_4 \tag{1}$$

where the adjustment factor F_1 depends on the relative orientation of joints and slope. F_2 refers to joint dip angle. F_3 reflects the relationship between slope and joints dips. F_4 is the adjustments factor related to excavation method; the value is 15 for natural slope. Table 1 shows how the SMR value is obtained for the studied slope. The input ratings are selected as the synthesized values of the metamorphic sandstone and the granite, considering the frequent existence of intrusive dikes.

The Q classification is another commonly used rock mass quality index. The Q -system was originally developed for underground excavations and has been applied to slopes as well (Pantelidis 2009). The numerical value of Q index is determined as follows:

$$Q = \frac{RQD J_r J_w}{J_n J_a SRF} \tag{2}$$

where J_n is the rating accounting for the number of joint sets, J_r is the rating related to joint surface roughness, J_a is the rating indicating the degree of joint alteration, J_w is the rating accounting for groundwater pressure and SRF is the

Table 1 SMR for the studied slope according to Romana (1985)

UCS (MPa)	73
Rating	7
RQD (%)	17.6
Rating	3
Discontinuous spacing (m)	0.1–0.6
Rating	9
Discontinuous conditions	sm to r, sw to mw, $s < 1.0$ mm
Rating	19
Groundwater	dry
Rating	15
Adjust factor F_1	Fair
Rating	0.7
Adjust factor F_2	Fair
Rating	0.7
Adjust factor F_3	unfavorable
Rating	–50
Adjust factor F_4	Natural slope
Rating	15
RMR	53
SMR	44

sm smooth, r rough, sw slightly weathered, mw moderately weathered, s joint separation

stress reduction rating representing the influence of in situ stress. Table 2 presents the Q index value and the selection of input ratings.

The GSI system was proposed by Hoek (1994) and Hoek et al. (1995) based on visual impression of rock structure. The system was mainly applied to slopes and open excavations. The GSI index was estimated from rock mass structure and joint surface condition. Sonmez and Ulusay (1999) provided a more rigorous method to determine the GSI value by introducing surface condition and structure ratings. This modified GSI geomechanical classification was used in this paper. During GSI value estimation, the

moderately weathered and crushed granite dikes were considered as weak layers in metamorphic sandstone rock mass. Table 3 illustrates how the GSI value is obtained.

Rock mass properties

The rock mass deformation modulus and strength are fundamental inputs for numerical modeling. Rock mass classifications are helpful in estimating these parameters. Several authors have presented empirical relationships between rock mass properties and geomechanical classification indices. Bieniawski (1989) provided corresponding friction angles and cohesions for RMR values. The relationship between deformation modulus of rock mass and RMR value for RMR < 50 is as follows:

$$E_m = 10^{(RMR-10)/40} \quad (3)$$

where E_m is the in situ modulus of deformation in GPa. These relations can also be used for the SMR values. The rock mass properties obtained by SMR index are shown in Table 4.

Barton (2002) suggested an equation for calculating E_m based on the normalisation of Q value as follows:

$$E_m = 10Q_c^{1/3} \quad (4)$$

Q_c is the normalization of the Q value, which is given as below:

$$Q_c = Q \cdot \frac{\sigma_c}{100} \quad (5)$$

where σ_c is the uniaxial compression strength.

Barton (2002) also proposed the below equations for calculating the friction angle f and cohesion c :

$$f = \tan^{-1} \left(\frac{J_r}{J_a} \cdot J_w \right) \quad (6)$$

$$c = \frac{RQD}{J_n} \frac{1}{SRF} \frac{\sigma_c}{100} \quad (7)$$

Table 2 Q index for the studied rock mass (Barton 2002)

RQD (%)	17.6
Joint set number	Four or more joint sets, heavily jointed
J_n	15
Joint roughness number	Smooth to rough, undulating, crushed zone
J_r	1.5
Joint alteration number	Unaltered joint walls to low friction mineral clay coating
J_a	2.5
Water reduction factor	Dry
J_w	1
Stress reduction factor	Low stress, near surface
SRF	2.5
Q value	0.32

Table 3 Geological strength index (GSI) for the study (Sonmez and Ulusay 1999)

Description	Blocky/disturbed: folded and/or faulted with angular blocks formed by many intersecting discontinuity sets
Size of blocks	Small to very small
Volumetric joint count, J_v (joint/m ³)	30
Structure rating, SR (%)	25
Surface condition rating (SCR)	
R_r	1
R_w	4
R_f	2
SCR	7
GSI	30

The deformation modulus and strength parameters obtained by Q value are given in Table 4. The uniaxial compression strength of the rock was chosen as the mean value of metamorphic sandstone and granite, 73 MPa.

For rock mass with $\sigma_c < 100$ MPa, Hoek et al. (2002) found a correlation between E_m and GSI:

$$E_m = \left(1 - \frac{D}{2}\right) \sqrt{\frac{\sigma_c}{100}} \cdot 10^{\left(\frac{GSI-10}{40}\right)} \tag{8}$$

where D is the disturbance factor that reflects the effects of blast damage or stress relaxation. For the friction angle f and cohesion c , the following equations were presented:

$$f = \sin^{-1} \left[\frac{6am_b(s + m_b\sigma_{3n})^{a-1}}{2(1+a)(2+a) + 6am_b(s + m_b\sigma_{3n})^{a-1}} \right] \tag{9}$$

$$c = \frac{\sigma_c[(1+2a)s + (1-a)m_b\sigma_{3n}](s + m_b\sigma_{3n})^{a-1}}{(1+a)(2+a) \sqrt{1 + \left[\frac{6am_b(s + m_b\sigma_{3n})^{a-1}}{2(1+a)(2+a)} \right]^2}} \tag{10}$$

where a , s and m_b are constants and can be obtained by the below equations:

$$a = \frac{1}{2} + \frac{1}{6} \left(e^{-GSI/15} - e^{-20/3} \right) \tag{11}$$

$$s = \exp\left(\frac{GSI - 100}{9 - 3D}\right) \tag{12}$$

$$m_b = m_i \exp\left(\frac{GSI - 100}{28 - 14D}\right) \tag{13}$$

where m_i is the Hoek–Brown intact material constant.

For slopes, σ_{3n} is calculated by following equation:

$$\sigma_{3n} = 0.72 \left(\frac{\sigma_{cm}}{\gamma H} \right)^{-0.91} \cdot \frac{\sigma_{cm}}{\sigma_c} \tag{14}$$

$$\sigma_{cm} = \sigma_c \cdot \frac{(m_b + 4s - a(m_b - 8s))(m_b/4 + s)^{a-1}}{2(1+a)(2+a)} \tag{15}$$

where γ is material density, H is slope height.

As we mentioned above, the granite dike was considered as weak layers in metamorphic sandstone mass during GSI estimation. The uniaxial compression strength used in Eqs. (14) and (15) was selected as the value of metamorphic sandstone. The Hoek–Brown intact material constant m_i was estimated to be 19 from published literature for competent rocks (Hoek and Brown 1997; Marinos and Hoek 2000). The mean front slope height is about 230 m and the rock mass density is 2600 kg/m³. Hoek et al. (2002) mentioned that zero disturbance factor results in more optimistic rock mass properties for undisturbed slope. The studied slope has a large unloading range (the horizontal unloading depth is about 180 m at a slope height of 200 m). The stress relief should be considered in estimating the parameters. In this paper, the disturbance factor D of 0.5 was assumed to account for effect of deep unloading. The rock mass properties obtained from GSI are shown in Table 4.

Table 4 Rock mass properties obtained by different classification system

References	Classification system	Frictional angle (°)	Cohesion (MPa)	Young’s modulus (GPa)
Bieniawski (1989)	SMR	27	0.22	7.1
Barton (2002)	Q	31	0.39	6.2
Hoek et al. (2002)	GSI	36	1.0	2.2
Average		31.3	0.54	5.2

The shear modulus G and bulk modulus K , which were used in numerical modeling, can be obtained from the deformation modulus E_m and Poisson's ratio ν :

$$G = \frac{E_m}{2(1 + \nu)} \quad (16)$$

$$K = \frac{E_m}{3(1 - \nu)} \quad (17)$$

The calculated shear modulus and bulk modulus are shown in Tab. 5. The deformation modulus of the rock mass was selected as the mean value of the different methods.

Stability analysis

General method

Kinematic, limit equilibrium and numerical simulation techniques were used for the slope stability analysis. First, the kinematic analysis was adopted to access the possible slope failure modes. The kinematic analysis results can provide useful information for further analysis. Then, the limit equilibrium method was utilized to obtain the factor of safety and the probability of failure for kinematically unstable blocks. Kinematic and limit equilibrium analyses can only consider a simplified model, so numerical modeling was also employed to study the deformation, stress distribution and yield status of the slope in detail. The failure behavior and failure mechanism of the slope were investigated using a discontinuum model with the aim of reflecting the slope morphology and tectonic effect. The discontinuum method has been a routine approach in stability analysis of rock slope controlled by joint-bounded blocks (Stead et al. 2006).

Kinematic stability analysis

Kinematic analysis based on stereographic projections was carried out on the potential slope failure controlled by discontinuities and slope orientation. The slope was considered as a whole and the average slope orientation of N140°/40° was used for kinematic analysis. Combinations of discontinuity orientations and slope face were examined to ascertain different possible modes of failure, such as planar, wedge and toppling failures, based on the criteria defined by Hoek and Bray (1981) and Goodman (1989). We used a direction tolerance of 30° for toppling failure. The lowest value of the friction angle of 27°, obtained by SMR technique (refer Table 4), was used in order to be more conservative. The commercial graphical and statistical analysis

software Dips (Rocscience 2012) was used for kinematic analysis.

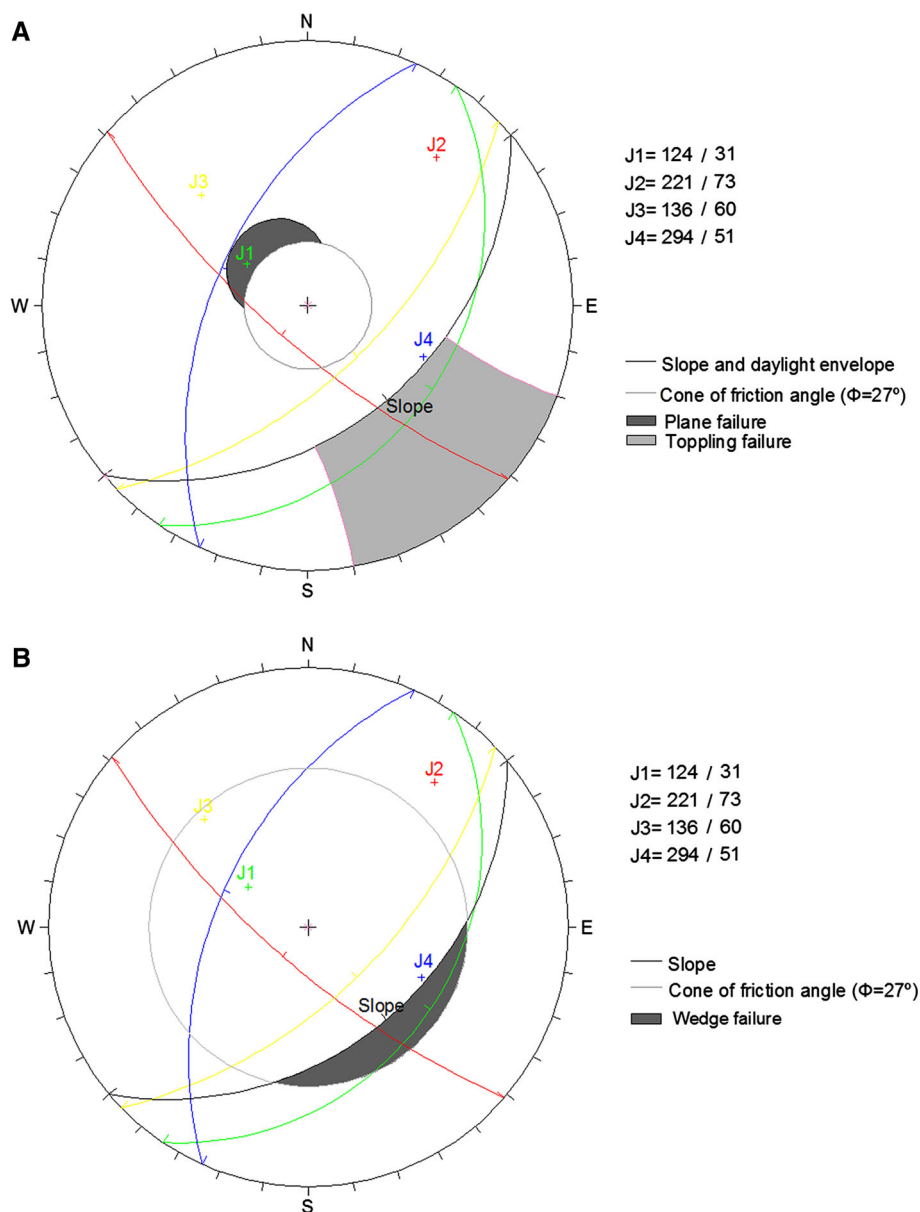
Kinematic analysis indicates that planar failure along J_1 is feasible in the study area (Fig. 7a). Although the mean orientation of joint set J_4 is out of the toppling failure envelope, there is a possibility of toppling failure along J_4 , taking into account the variability of orientation, especially in the place with steep slope angle. We did find some toppling failure at the toe of the slope where the slope angle is greater than 50°, but no field evidence of widespread toppling was observed at higher elevation of the slope. Toppling along the bedding plane may result in separation of J_3 and weakening of the strength of the rock mass at the toe, which then provide feasibility to planar failure along J_1 . Figure 7b highlights that the wedge failure is kinematically possible along the plunge of the intersection of J_1 and J_2 .

Probabilistic analysis

The factor of safety for the kinematically feasible planar failure along J_1 and wedge failure along the plunge of intersection of J_1 and J_2 was calculated based on the limit equilibrium analysis. The analyses were carried out with Rocplane (Rocscience 2003) and Swedge (Rocscience 2002). The stability methods given by Hoek and Bray (1981) were used to evaluate the possibility of planar and surface wedge failures. The slope was still considered as a whole and no cohesive strength was considered for the discontinuities. For a deterministic analysis, only representative values were used. However, the strength values suggested by classification system include high uncertainty since they were obtained from a large amount of statistical data. Therefore, the probabilistic analysis method was accomplished along with deterministic analysis. The representative value of friction angle in deterministic analysis and the mean value in the probabilistic analysis were chosen as the average value of the three classification systems (refer to Table 5), i.e., 31.3°. The coefficient of variation was chosen as 10 % according to the experience of Park and West (2001). A narrow range within three standard deviations of mean value was assumed (Rethai 1998). The Monte Carlo simulation was adopted for the probabilistic analysis and 1000 samples were generated in this study.

The deterministic analysis indicated that the factors of safety for planar failure along joint set J_1 and wedge failure along joint sets J_1 and J_2 are 1.03 and 1.17, respectively. They stand for different stability status. The slope is nearly in a critical equilibrium status for planar failure along joint set J_1 . The planar failure can occur at any moment. However, the slope is relatively safe when considering the

Fig. 7 Kinematic analysis for different modes of failures: **a** planar and toppling failure and **b** wedge failure



wedge failure. Probabilistic analyses gave similar results. The histogram of safety factors in Fig. 8 shows that the probability of instability is 43.1 % for planar failure along joint set J_1 . This value is much higher than the probability of wedge failure for the combination of J_1 and J_2 , which is only 10.7 %. Therefore, the planar failure along joint sets J_1 represents a frequent and common failure mechanism at Xiari slope. However, we must keep in mind that the calculated mean block volume of wedge failure, although has a very low possibility, reaches $4.7 \times 10^6 \text{ m}^3$, which is much larger than that of planar failure, $1.4 \times 10^4 \text{ m}^3$. This indicates that the wedge failure stands for a greater hazard.

Considering the poor quality of the rock mass, circular slip surface analyses were also carried out to examine

whether the slope has the possibility of non-discontinuities controlled failure. The 2D limit equilibrium slope stability analysis software Slide (Rocscience 2010) was used, and Bishop, Janbu Corrected and Spencer analysis methods were adopted. The three subareas of the slope were evaluated separately because of different topographies. The locations of profiles are shown in Figs. 1 and 3. In order to eliminate the influence of the covering soils, high strength parameters were given to the soils. The friction angle and cohesion of the rock mass were selected as random variables. The mean values of these parameters are shown in Table 5. Also, the coefficient of variation was chosen as 10 % and the random samples were generated by Monte Carlo simulation and fell within three standard deviations

of the mean values. The geometric models of the three subareas and the results determined by the Spencer method are shown in Fig. 9a–c. The results illustrate that all three subareas of the slope have deep-seated failure modes. The mean factor of safety ranges from 1.696 (Janbu Corrected method) to 1.705 (Bishop method) for subarea A, 1.672 (Spencer method) to 1.679 (Janbu Corrected method) for subarea B and 1.575 (Spencer method) to 1.577 (Bishop

Table 5 Rock mass properties used in modeling analysis

Density (kg/m^3)	2600
Uniaxial compressive strength (MPa)	73
Young's modulus for intact rock (GPa)	35
Tensile strength (MPa)	0.015
Young's modulus (GPa)	5.2
Poisson's ration	0.25
Cohesion (MPa)	0.54
Friction angle ($^\circ$)	31.3
Bulk modulus (GPa)	3.4
Shear modulus (GPa)	2.0

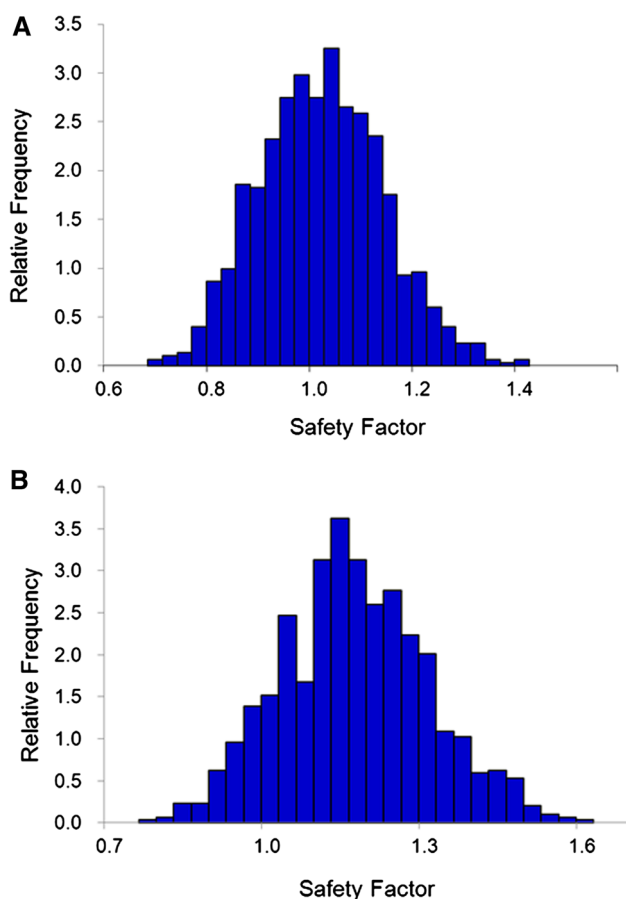


Fig. 8 Histogram of factor of safety for: **a** planar failure and **b** wedge failure calculated in probabilistic analysis

method) for subarea C. It indicates that there is no probability of slope failure with circular slip surface during current conditions.

Discontinuum analysis

In order to study the deformation behavior of the structurally controlled rock slope, discontinuum modeling was carried out using the two-dimensional distinct element code UDEC (Itasca 2005). The profile sections considered for the numerical modeling are shown in Fig. 3. The joint planes of different joint sets were generated based on average apparent dip values from field measurements. However, joint set J_2 was not included since its trend is nearly parallel to the profile trend. The spacing of the joints needed to be increased for the feasibility of modeling. The rock block was modeled using linearly elastic model and discontinuities were modeled using an elasto-plastic model with Mohr–Coulomb failure criterion. The joint stiffness was estimated using the elastic modulus of rock mass and intact rock blocks from the following expressions (Itasca 2005):

$$k_n = \frac{E_m E_i}{s(E_i - E_m)} \quad (18)$$

$$k_s = \frac{G_m G_i}{s(G_i - G_m)} \quad (19)$$

where k_n is the joint normal stiffness, k_s is the joint shear stiffness, E_m is the rock mass Young's modulus, E_i is the intact rock Young's modulus, G_m is rock mass shear modulus, G_i is intact rock shear modulus, s refers to joint spacing.

The strength parameters of discontinuities used the mean parameters obtained by the rock classification systems. The high cohesion was utilized to model the non-persistent effect of the joints. Relatively lower strength was used for J_3 to consider the tectonic and unloading effect. The physical and mechanical parameters of the discontinuities are given in Table 6. The properties of covering soil obtained by physical and direct shear tests are shown in Table 7. In-situ stress information has not been measured in the study area. According to the work in the same tectonic unit (Qi et al. 2004; Gong et al. 2010; Huang et al. 2011), the horizontal tectonic stress of 10.0 MPa for rock mass was used in the numerical model.

The surface soil is thin and has little influence on the stability of the entire slope. Therefore, we only emphasized on the stability of the rock mass. The results of the numerical modeling showed that the profile sections in three different subareas of Xiari slope have different stability and deformation mechanisms. In subarea A, the prehistoric landslide significantly changed the stress state

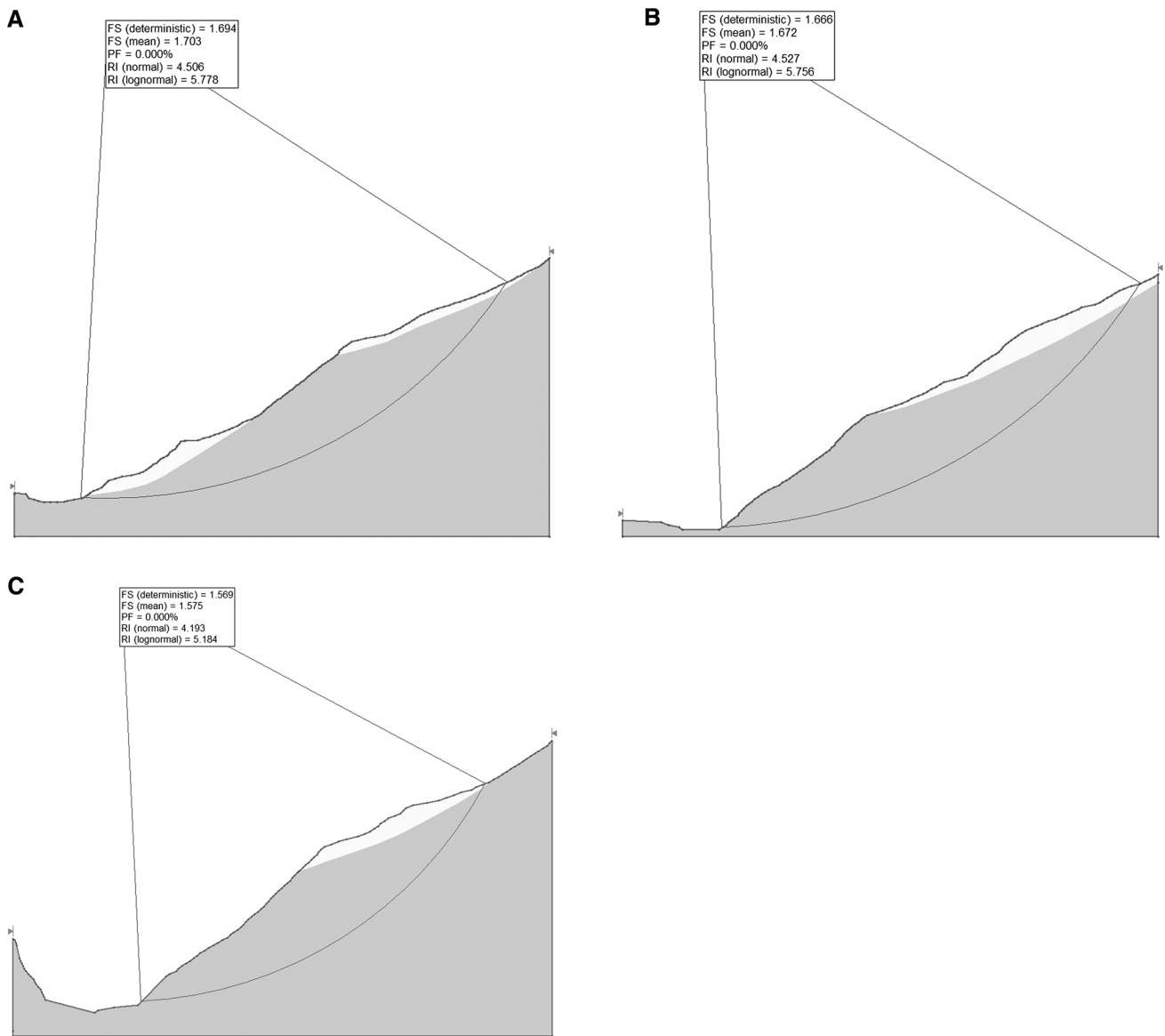


Fig. 9 Circular slip surface results of deterministic and probabilistic analyses for subareas **a** A, **b** B and **c** C using the Spencer method

Table 6 Discontinuity properties used in modeling analysis

Discontinuities	J_1	J_3	J_4
Apparent dip (°)	30	59	-48
Spacing (m)	20	20	25
Cohesion (MPa)	0.54	0.22	0.54
Friction angle (°)	31.3	27	31.3
Joint normal stiffness (GPa/m)	19	19	19
Joint shear stiffness (GPa/m)	7	7	7

of the frontal slope. It indicates that the shear stress decreased at the foot and increased on the middle of the slope (Fig. 10a). The landslide deposit at the toe acts as a resistance to future rock slope failure. Numerical modeling

Table 7 Soil properties used in discontinuum modeling

Density (kg/m ³)	2020
Friction angle (°)	26
Cohesion (kPa)	45
Bulk modulus (MPa/m)	45
Shear modulus (MPa/m)	15

shows that the condition for developing continuous basal failure surface can't be met at present. Thus, the rock slope in subarea A is more stable. In subarea B, shear strain concentrated at the foot of the rock slope (Fig. 10b), but there is no continuous basal failure surface through the toe that developed. This part is also stable at present stage. Numerical modeling in Fig. 10c highlights that subarea C

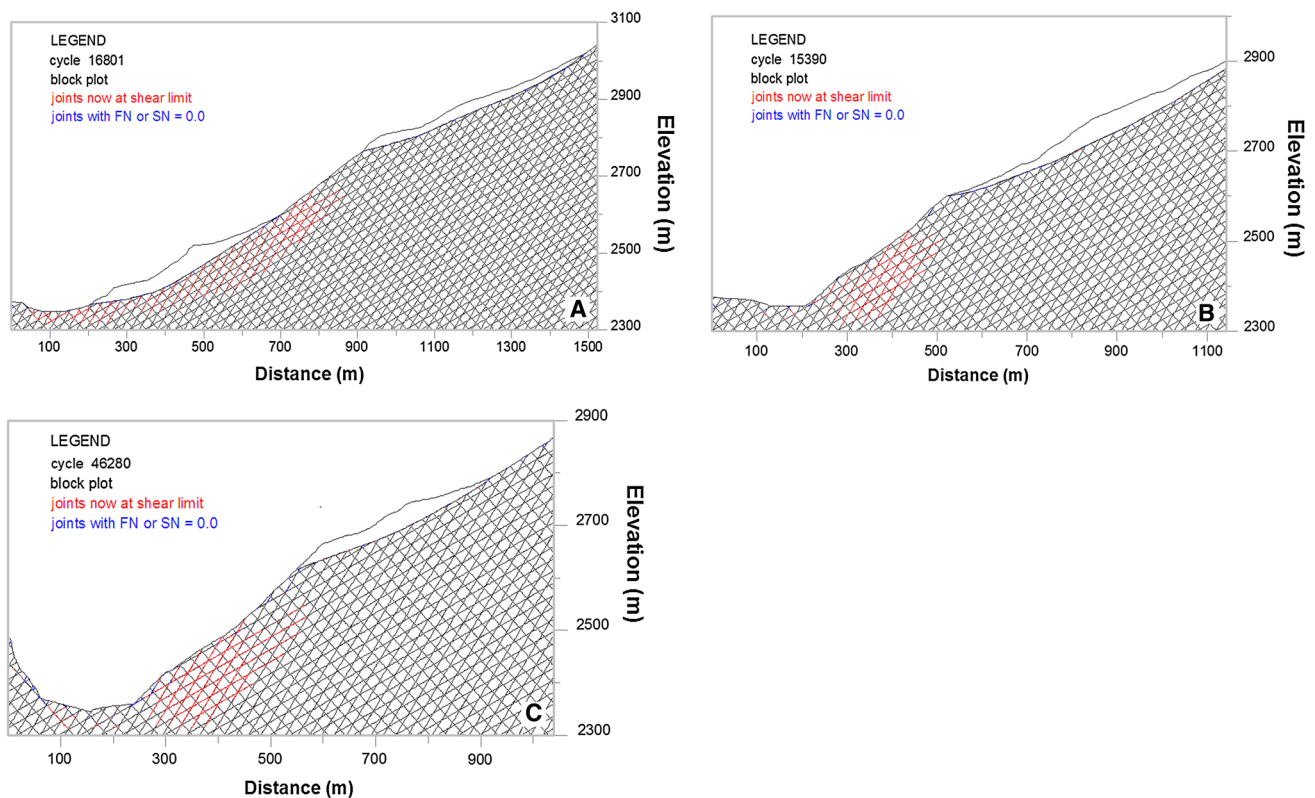


Fig. 10 Discontinuum modeling results for the subareas: **a** A, **b** B and **c** C. Refer to Figs. 1 and 3 for profile sections (*FN* normal stress, *SN* shear stress)

is prone to be unstable. The specific discontinuity configuration on the studied profile is characterized for a large rockslide. Continuous basal failure surfaces through the toe can develop along joint J_1 , which reached its shear limit. These, combined with the rear failure surfaces developed along the steep joint J_3 , can meet the needs for the occurrence of a landslide. It also should be considered that the joint J_2 , which wasn't included in the numerical modeling, may form the lateral detachment structures. The potentially unstable block was estimated to be more than $2.5 \times 10^6 \text{ m}^3$. The unstable volume was estimated from Fig. 10c and the dimension of subarea C. There is no toppling mode of failure in the three studied profiles. Some open joints along J_3 in combination with the shear joint along J_1 near the frontal surfaces may explain the detachment of isolated blocks as a source of rock avalanche.

Discussion

The narrow valley, downstream to the Xiari slope, is an ideal place for dam construction. But the possible failure of this slope is a great threat to potential construction. Due to the high concerns and high risk, it is important to answer questions about the likelihood of slope failure. The Xiari potentially unstable rock slope would be structurally

controlled. Based upon kinematic and limit equilibrium analyses, planar and wedge failures seem to be the two main potential failure mechanisms. Planar failure has a higher probability of occurrence as compared to wedge failure. However, it needs to be remembered that the kinematic models are simplified and might be different from reality. The Xiari slope has a complex topography. Field observation shows that the failure mechanism of a large landslide highly depends on the combination of topography and discontinuities rather than on discontinuities alone. The deep and steep erosional gully developed in the upstream of subarea A is an important factor for prehistoric landslide failure, which provided a favorable outlet for the landslide. With the development of the erosional gully in the upstream of subarea C, a large catastrophic landslide like that in subarea A is possible. However, this complex failure mechanism is difficult to be modeled in the 2D numerical model. A 3D numerical model would probably improve our understanding of the entire slope's instability.

Conclusion

Detailed field survey and different analysis methods were adopted to understand the stability and potential failure mechanism of the Xiari rock slope. The slope stability in the

study area is strongly controlled by a combination of slope topography and discontinuities. Tectonic movement and the unloading effect weaken the shear strength of the discontinuities. The unfavorable integration of discontinuities and frontal scarp may result in potential failure of rock slope.

Kinematic analysis indicates that the potential failure modes are planar and wedge failure, while large scale toppling failure is unlikely in this area. Planar failure along joint J_1 is almost certain to occur in this area. The collapses of planar failure would have small size, with mean volume of $1.4 \times 10^4 \text{ m}^3$, as observed through the analysis. These failures usually cannot reach down to the bottom of the valley and thus have minor hazards. On the other hand, the large-sized wedge failures, with mean calculated volume of $4.7 \times 10^6 \text{ m}^3$, pose high hazard.

Numerical modeling indicates that subareas A and B are not prone to large failures at present. But subarea C has a high risk of failure. The suitable discontinuity configuration combined with the topography might result in a catastrophic failure, such as the prehistoric one in subarea A. The potential failure blocks are estimated to be more than $2.5 \times 10^6 \text{ m}^3$ by numerical modeling. The volume is large enough to cause tsunamis in the water reservoir and block the river, and hence poses a great threat to nearby construction and villages.

Acknowledgments The authors would like to gratefully acknowledge the financial support provided by the National Natural Science Foundation of China (No. 41272328).

References

- Barton N (2002) Some new Q-value correlations to assist in site characterization and tunnel design. *Int J Rock Mech Min Sci* 39:185–216
- Bieniawski ZT (1973) Engineering classification of jointed rock masses. *Trans South Afr Inst Civil Eng* 15(12):335–344
- Bieniawski ZT (1989) *Engineering rock mass classifications*. Wiley, New York
- Böhme M, Hermanns RL, Oppikofer T, Fischer L, Bunkholt HSS, Eiken T, Pedrazzini A, Derron M-H, Jaboyedoff M, Blikra LH, Nilsen B (2013) Analyzing complex rock slope deformation at Stampa, western Norway, by integrating geomorphology, kinematics and numerical modeling. *Eng Geol* 154:116–130
- Dai F, Lee C, Deng J, Tham L (2005) The 1786 earthquake-triggered landslide dam and subsequent dam-break flood on the Dadu River, southwestern China. *Geomorphology* 65:205–221
- Deere DU (1989) Rock quality designation (RQD) after twenty years. U.S. Army Corps of Engineers Contract Report GL-89-1. Waterways Experiment Station, Vicksburg, MS 67
- Genis M, Basarir H, Ozarslan A, Bilir E, Balaban E (2007) Engineering geological appraisal of the rock masses and preliminary support design, Dorukhan Tunnel, Zonguldak, Turkey. *Eng Geol* 92:14–26
- Gong M, Qi S, Liu J (2010) Engineering geological problems related to high geo-stresses at the Jinping I Hydropower Station, Southwest China. *Bull Eng Geol Environ* 69:373–380
- Goodman RE (1989) *Introduction to rock mechanics*. Wiley, New York
- Gurocak Z, Alemdag S, Zaman MM (2008) Rock slope stability and excavatability assessment of rocks at the Kapikaya dam site, Turkey. *Eng Geol* 96:17–27
- Hoek E (1994) Strength of rock and rock masses. *ISRM News J* 2(2):4–16
- Hoek E, Bray J (1981) *Rock slope engineering*, 3rd edn. E & FN Spon, London
- Hoek E, Brown E (1997) Practical estimates of rock mass strength. *Int J Rock Mech Min Sci* 34:1165–1186
- Hoek E, Kaiser P, Bawden W (1995) *Support of underground excavations in hard Rock*. Balkema, Rotterdam, p 215
- Hoek E, Carranza-Torres C, Corkum B (2002) Hoek–Brown failure criterion—2002 Edition. In: *Proceedings of NARMS-TAC conference*, Toronto, pp 267–273
- Huang RQ (2009) Some catastrophic landslides since the twentieth century in the southwest of China. *Landslides* 6:69–81
- Huang R, Fan X (2013) The landslide story—nature geo. *Nat Geosci* 6:2
- Huang R, Wang Y, Wang S, Li Y (2011) High geo-stress distribution and high geo-stress concentration area models for eastern margin of Qinghai-Tibet plateau. *Sci China Technol Sci* 54:154–166
- ISRM (1981) *Rock characterization, testing and monitoring*. In: Brown ET (ed) *ISRM suggested methods*. Pergamon Press, New York
- Itasca (2005) *UDEC-universal distinct element code: user's guide*. Itasca Consulting Group, Minneapolis
- Justo J, Justo E, Azañón J, Durand P, Morales A (2009) The use of rock mass classification systems to estimate the modulus and strength of jointed rock. *Rock Mech Rock Eng* 43:287–304
- Marinos P, Hoek E (2000) GSI: A geologically friendly tool for rock mass strength estimation. In: *Proceedings of GeoEng2000 conference*, Melbourne, pp 1422–1442
- Palmstrom A (2005) Measurements of and correlations between block size and rock quality designation (RQD). *Tunn Undergr Space Technol* 20:362–377
- Pantelidis L (2009) Rock slope stability assessment through rock mass classification systems. *Int J Rock Mech Min Sci* 46:315–325
- Park H, West T (2001) Development of a probabilistic approach for rock wedge failure. *Eng Geol* 59:233–251
- Qi S, Wu F, Yan F, Lan H (2004) Mechanism of deep cracks in the left bank slope of Jinping first stage hydropower station. *Eng Geol* 73:129–144
- Rethai L (1998) *Probabilistic solutions in geotechnics*. Elsevier, Amsterdam
- Rocscience (2002) *Swedge v5.0-Probabilistic analysis of the geometry and stability of surface wedges*. Rocscience Inc., Canada
- Rocscience (2003) *RocPlane v2.0-Planar sliding stability analysis for rock slopes*. Rocscience Inc., Canada
- Rocscience (2010) *Slide v6.0-2D limit equilibrium slope stability analysis*. Rocscience Inc., Canada
- Rocscience (2012) *Dips v6.0-Graphical and Statistical Analysis of Orientation Data*. Rocscience Inc., Canada
- Romana M (1985) New adjustment ratings for application of Bieniawski classification to slopes. In: *Proceedings of the international symposium on the role of rock mechanics in excavations for mining and civil works*. International Society of Rock Mechanics, Zacatecas, pp 49–53
- Sonmez H, Ulusay R (1999) Modifications to the geological strength index (GSI) and their applicability to stability of slopes. *Int J Rock Mech Min Sci* 36:743–760
- Stead D, Eberhardt E, Coggan J (2006) Developments in the characterization of complex rock slope deformation and failure using numerical modelling techniques. *Eng Geol* 83:217–235

- Wen B, Wang S, Wang E, Zhang J (2004) Characteristics of rapid giant landslides in China. *Landslides* 1:247–261
- Wu S, Shen M, Wang J (2010) Jinping hydropower project: main technical issues on engineering geology and rock mechanics. *Bull Eng Geol Environ* 69:325–332
- Xu W, Xu Q, Wang Y (2013) The mechanism of high-speed motion and damming of the Tangjiashan landslide. *Eng Geol* 157:8–20
- Yin Y, Wang F, Sun P (2009) Landslide hazards triggered by the 2008 Wenchuan earthquake, Sichuan, China. *Landslides* 6:139–152
- Zhou J, Xu W, Yang X, Shi C, Yang Z (2010) The 28 October 1996 landslide and analysis of the stability of the current Huashiban slope at the Liangjiaren Hydropower Station, Southwest China. *Eng Geol* 114:45–56